Carbohydrate Polymers 90 (2012) 948–956

Contents lists available at SciVerse ScienceDirect

Carbohydrate Polymers

journal homepage: www.elsevier.com/locate/carbpol

Effects of modified cellulose nanocrystals on the barrier and migration properties of PLA nano-biocomposites

E. Fortunati[a,*], M. Peltzer[c], I. Armentano[a], L. Torre[a], A. Jiménez[c], J.M. Kenny[a,b]

[a] Materials Engineering Center, UdR INSTM, University of Perugia, Italy
[b] Institute of Polymer Science and Technology, CSIC, Spain
[c] University of Alicante, Department of Analytical Chemistry, Nutrition and Food Sciences, P.O. Box 99, 03080 Alicante, Spain

ARTICLE INFO

Article history:
Received 16 April 2012
Received in revised form 17 May 2012
Accepted 10 June 2012
Available online 19 June 2012

Keywords:
Nano-biocomposites
Poly(lactic acid)
Cellulose nanocrystals
Barrier properties
Overall migration

ABSTRACT

The aim of this paper is to report the impact of the addition of cellulose nanocrystals on the barrier properties and on the migration behaviour of poly(lactic acid), PLA, based nano-biocomposites prepared by the solvent casting method. Their microstructure, crystallinity, barrier and overall migration properties were investigated. Pristine (CNC) and surfactant-modified cellulose nanocrystals (s-CNC) were used, and the effect of the cellulose modification and content in the nano-biocomposites was investigated.

The presence of surfactant on the nanocrystal surface favours the dispersion of CNC in the PLA matrix. Electron microscopy analysis shows the good dispersion of s-CNC in the nanoscale with well-defined single crystals indicating that the surfactant allowed a better interaction between the cellulose structures and the PLA matrix. Reductions of 34% in water permeability were obtained for the cast films containing 1 wt.% of s-CNC while good oxygen barrier properties were detected for nano-biocomposites with both 1 wt.% and 5 wt.% of modified and un-modified cellulose nanocrystals, underlining the improvement provided by cellulose on the PLA films. Moreover, the migration level of the studied nano-biocomposites was below the overall migration limits required by the current normative for food packaging materials in both non-polar and polar simulants.

1. Introduction

Production of innovative "green materials" derived from natural sources is currently one of the main points of interest in the academic and industrial areas of material research. Studies based on nano-biocomposites using different reinforcements for poly(lactic acid), PLA, have been reported by many research groups in recent years (Fortunati, Armentano, Zhou, Iannoni, et al., 2012; Petersson, Kvien, & Oksman, 2007; Sanchez-Garcia, Gimenez, & Lagaron, 2008). PLA is a biodegradable thermoplastic polyester produced from L- and D-lactic acid, which is obtained from the fermentation of corn starch. PLA is currently commercialized and used in food packaging application for fresh or relatively short shelf-life products as containers, drinking cups, salad cups, overwrap and lamination films, and blister packages (Auras, Kale, & Singh, 2006; Schwach, Six, & Luc Averous, 2008). However, some drawbacks such as low thermal stability and poor barrier properties have reduced their application in food packaging. The addition of nanomaterials could be considered an adequate alternative to limit such problems and consequently to improve the possibilities for PLA based packages (Bordes, Pollet, & Averous, 2009; Martino, Jiménez, Ruseckaite, & Avérous, 2011). The use of cellulose nanowhiskers or nanocrystals has been proposed as the load-bearing constituent in developing new and inexpensive bio-materials due to their high aspect ratio, good mechanical properties and fully degradable and renewable character (Sturcova, Davies, & Eichhorn, 2005). If compared to other inorganic reinforcing fillers for biopolymers, cellulose nanocrystals have some additional advantages, including their wide availability of sources, low-energy consumption, ease of recycling including combustion, high sound attenuation and comparatively easy processability due to their non-abrasive nature, allowing high filling levels and significant cost savings (Samir & Dufresne, 2005). The use of cellulose nanocrystals as nano-reinforcements is an emerging field in nanotechnology, but there are still some obstacles for their use. Firstly, cellulose nanocrystals are not commercially available since their production is still associated with low yields. In addition, they are difficult to use with water insoluble polymers like PLA, because their high ability to produce strong hydrogen bonding. Therefore, cellulose nanocrystals have to be transferred from water to an appropriate solvent in order to produce and process PLA composite systems (Araki, Wada, & Kuga, 2001; Goussé, Chanzy, Cerrada, & Fleury, 2004; Heux, Chauve, & Bonini, 2000).

The control of the degradation rate and the release of potentially migrant compounds, are key issues for the design of biodegradable systems for food packaging. PLA is the most interesting

* Corresponding author at: Strada di Pentima 4, 05100, Terni, Italy. Tel.: +39 0744 492921; fax: +39 0744 492950.
E-mail address: elena.fortunati@unipg.it (E. Fortunati).

0144-8617/$ – see front matter © 2012 Elsevier Ltd. All rights reserved.
http://dx.doi.org/10.1016/j.carbpol.2012.06.025

biopolymer for manufacturing these materials, and consequently it should be prepared to be in contact with different types of food (Mutsuga, Kawamura, & Tanamoto, 2008). Lactic acid is the lone monomer in the PLA structure but migrants in PLA based systems could be lactic acid itself joined to dimmers and other oligomers, produced by the PLA hydrolysis (Jamshidian, Tehrany, Imran, Jacquot, & Desobry, 2010). However, different results could be found for PLA blends, composites and copolymers, with more complex migration processes. In general, food packaging materials should be designed to control the gas permeability and to minimize migration of additives and other compounds during storage or processing.

The aim of this research is to study the impact of cellulose nanocrystals derived from highly purified cellulose fibres on the properties of PLA nano-biocomposites, with special focus on the barrier properties and on their interaction with food simulants.

2. Experimental

2.1. Materials

Poly(lactic acid), PLA 3051D, with specific gravity 1.25 g cm^{-3}, molar mass of ca. 1.42×10^4 g mol^{-1}, and melt flow index (MFI) 7.75 g 10 min^{-1} (210 °C, 2.16 kg) was supplied by Nature Works® (Minnetonka, MN, USA). PLA pellets were dried in a vacuum oven at 98 °C for 3 h. Microcrystalline cellulose (MCC, dimensions 10–15 μm) was supplied by Sigma–Aldrich (Milan, Italy).

2.2. Cellulose nanocrystals synthesis and modification

MCC was hydrolyzed in sulphuric acid hydrolysis (64%, wt/wt) at 45 °C for 30 min following the recipe reported by Cranston and Gray (2006). After acid remotion, dialysis and ultrasonic treatment, the resultant cellulose nanocrystal aqueous suspension was approximately 0.5% by weight and the yield was ca. 20%. Furthermore, mixed bed ion exchange resin (Dowex Marathon MR-3 hydrogen and hydroxide form) was added to the cellulose suspension for 48 h and then removed by filtration. CNC suspension was neutralized by the addition of 1.0% (v/v) 0.25 mol L^{-1} NaOH (Wang, Ding, & Cheng, 2007). The synthesized nanocrystals were then examined by transmission electron microscope (TEM, Philips Tecnai 10) operated at an acceleration voltage of 80 kV after the deposition of a droplet of dilute CNC suspension (0.1 wt.%) on a bacitracin pre-treated surface of a carbon-coated grid.

Modified cellulose nanocrystals (s-CNC) were obtained with an acid phosphate ester of ethoxylated nonylphenol (Beycostat A B09 (CECCA S.A.)) in a 1/4 (wt/wt) ratio (Heux et al., 2000). The pH of the suspension was then fixed to 8.5 by using the same 0.25 wt.% NaOH solution.

After freeze drying, chloroform was directly added to the cellulose powder (both pristine CNC and s-CNC) forming 1 wt.% suspensions. In order to improve the cellulose dispersion in chloroform, the suspensions were exposed to sonication (Vibracell, 750) for 1 min in an ice bath. The morphological features of the modified nanocrystals after the dispersion in the organic solvent were investigated by using field emission scanning electron microscopy (FESEM, Supra 25-Zeiss). Few droplets of dilute s-CNC suspension (0.1 wt.%) were deposited on a silicon wafer, gold sputtered and analysed. The flow birefringence properties of modified cellulose nanocrystals suspension in chloroform, at 0.6 wt.% concentration, were detected between crossed polars in a dark box. Pictures were taken with a Nikon D300s digital camera.

2.3. PLA nano-biocomposite processing

PLA nano-biocomposite films were prepared by the solvent casting method. PLA (1 g) was dissolved in 25 mL $CHCl_3$ with vigorous stirring at room temperature (RT). The dissolved solution was poured onto a 15 cm diameter glass Petri dish and then allowed to dry for about 24 h at RT. For the preparation of the nano-biocomposite films, a predetermined amount of s-CNC suspension in chloroform was mixed with the previously prepared PLA solution. The solutions were stirred for 4 h before they were cast onto the glass Petri dish. The resultant films with a thickness of ca. 40 μm were peeled from the Petri dish after drying.

Nano-biocomposites with 1 wt.% (PLA/1s-CNC) or 5 wt.% (PLA/5s-CNC) of s-CNC were prepared. For comparison, PLA/CNC films with 1 wt.% (PLA/1CNC) and 5 wt.% (PLA/5CNC) of un-modified CNC were produced by following the above-described procedure. All systems were placed in a vacuum oven at 40 °C for 2 weeks in order to remove all remaining chloroform.

2.4. PLA nano-biocomposite characterization

2.4.1. Microstructure and wide angle X-ray scattering (WAXS)

The microstructure of PLA nano-biocomposites and the filler dispersion in the matrix were investigated by using transmission electron microscope (TEM, JEOL JEM-2010). Samples for TEM analysis were previously ultra-microtomed (RMC, model MTXL) in order to obtain slices 100 nm thick.

Wide angle X-ray scattering (WAXS) patterns of PLA nano-biocomposite films were obtained by means a Seifert diffractometer (JSO-DEBYEFLEX 2002) with Cu Kα radiation (λ = 0.1546 nm), 40 kV voltage and 40 mA current. The diffraction intensities were recorded between 2° and 80° (2θ angle range) by steps of 1° min^{-1}.

2.4.2. Oxygen transmission rate (OTR) measurements

OTR was measured with an oxygen permeation analyzer (Systech instruments, model 8500, Metrotec S.A.). PLA and PLA nanocomposites with a 14 cm diameter were employed for each formulation. Film thickness was measured using a Digimatic Micrometer Series 293 MDC-Lite (Mitutoyo) to ±0.001 mm. Samples were clamped in the diffusion chamber at 25 ± 1 °C. Pure oxygen (99.9%) was introduced into the upper half of the sample chamber while nitrogen was injected into the lower half of the chamber where an oxygen sensor was placed.

2.4.3. Water vapour permeability (WVP) tests

Water vapour permeability (WVP, kg m m^{-2} s^{-1} Pa^{-1}) was determined according to UNE 53097:2002 standard and it was calculated as

$$\mathrm{WVP} = \frac{(\mathrm{WVT} \times e)}{\Delta P} \quad (1)$$

where WVT (kg s^{-1} m^{-2}) is the vapour transmission rate through a mean film thickness e (m) and ΔP is the actual difference in partial water vapour pressure between the two sides of the specimens (Pa).

95 mm diameter samples were fixed with paraffin on the top of aluminum capsules containing $CaCl_2$ as drying agent. The capsules were placed in a climate chamber at controlled temperature and relative humidity: 20.0 ± 0.1 °C and 50 ± 2% RH, respectively, and they were weighed periodically until the steady state was reached. The mass change (±0.0001 g) of these capsules versus time was recorded at specific intervals (t) and then plotted. Linear regression was used to calculate the slope of a fitted straight line, which represent the WVT as follows:

$$\mathrm{WVT} = \frac{\Delta m}{t \times A} \quad (2)$$

where Δm is the mass change of the capsule test (kg) at time t (s) and A is the test area (m^2). Permeability was then calculated according to the following equation:

$$\text{WVP}\ \ (\text{kg m}/(\text{m}^2\,\text{s Pa})) = \frac{\text{WVT}}{S \times (\text{RH}_1 - \text{RH}_2)} * e \quad (3)$$

where e is the film thickness (m), S is the saturation pressure (Pa) at the test temperature, RH_1 is the relative humidity of the climatic chamber and RH_2 is the relative humidity inside the capsule. At least three repetitions per experiment were performed as previously reported (Martucci & Ruseckaite, 2010).

2.4.4. Overall migration test

Overall migration tests were performed in two liquid food simulants: ethanol 10% (v/v) (simulant A) and isooctane (alternative simulant to D2), according to the Commission Regulation EU No 10/2011. Rectangular strips of 10 cm^2 total area of each film were immersed in a glass tube with 10 mL of food simulants. Samples in ethanol 10% were kept in a controlled chamber at 40 °C during 10 days, while samples in isooctane were kept at 20 °C during 2 days, according to EN-1186 standard. After the incubation period, the films were removed and simulants were evaporated to dryness. Furthermore, the residue was weighed with an analytical balance (Sartorius ATILON) with ±0.1 mg precision in order to determine the overall migration value in mg kg^{-1} of simulant. For each sample three determinations were performed and the final migration value was the average of the three determinations.

In order to analyze the effect of incubation on the PLA nano-biocomposite properties, their surface microstructure, before and after incubation in ethanol 10% (v/v), was investigated by scanning electron microscope, FESEM, Supra 25-Zeiss. Samples were sputtered with gold and then analyzed.

The thermal behaviour of PLA and PLA nano-biocomposites after 10 days of incubation in ethanol 10% (v/v) was studied in order to evaluate the effect of the simulant on the sample thermal properties. Thermogravimetric analysis (TGA, Seiko Exstar 6300) was performed with the following experimental conditions: 10 ± 1 mg samples in nitrogen atmosphere (250 mL min^{-1}), from 30 °C to 600 °C, heating rate 10 °C min^{-1}. Differential scanning calorimetry tests (DSC, Mettler Toledo 822e) were performed from −25 °C to 250 °C, at 2 °C min^{-1}, with consecutive heating, cooling and heating scans. Melting and cold crystallization temperatures and enthalpies (T_m, T_{cc}, ΔH_m, ΔH_{cc}) were determined from the first heating scan while glass transition temperatures (T_g) were evaluated from the second heating and cooling scans.

3. Results and discussion

3.1. Cellulose nanocrystals

The hydrolysis process allowed to obtain well individualized CNC with the typical dimensions ranging from 100 to 200 nm in length and 5–10 nm in width as previously reported (Fortunati, Armentano, Zhou, Iannoni, et al., 2012; Fortunati, Armentano, Zhou, Puglia, et al., 2012). Nevertheless, the dispersion and self-ordering properties of cellulose nanocrystals are restricted to aqueous suspensions or dispersions in a few specific organic solvents with high dielectric constant such as DMSO or ethylene glycol (Turbak, Snyder, & Sandberg, 1983). The main reason for such restriction is the high tendency to agglomeration of these nanocrystals in non-polar solvents caused by their electrostatic character and the loss of stability of their suspensions. In consequence, their adequate dispersion in organic solvents is difficult.

After the hydrolysis process, suspensions containing unmodified crystals (CNC) and surfactant modified cellulose (s-CNC), were freeze-dried and the cellulose powders were re-dispersed in chloroform. We have already reported the strategy to employ a surfactant to avoid aggregation and favour the dispersion of cellulose nanocrystals in chloroform (Fortunati, Armentano, Zhou, Puglia, et al., 2012). One example of a FESEM image of surfactant-modified cellulose nanocrystals dispersed in chloroform is reported in Fig. 1a. Results obtained for crystal shape and size highlighted that no particular morphological modifications occurred during the dispersion in the organic solvent and CNC maintained their original acicular structure.

Moreover, the flow birefringence properties of cellulose nanocrystal suspensions in $CHCl_3$ were investigated (Fig. 1b). Suspensions exhibited strong shear birefringence, highlighting the ability of nanocrystals to form a chiral nematic liquid crystalline phase in equilibrium with the isotropic phase (Fleming, Gray, & Matthews, 2001). The flow birefringence of modified nanocrystals in chloroform proved their good dispersion in chloroform

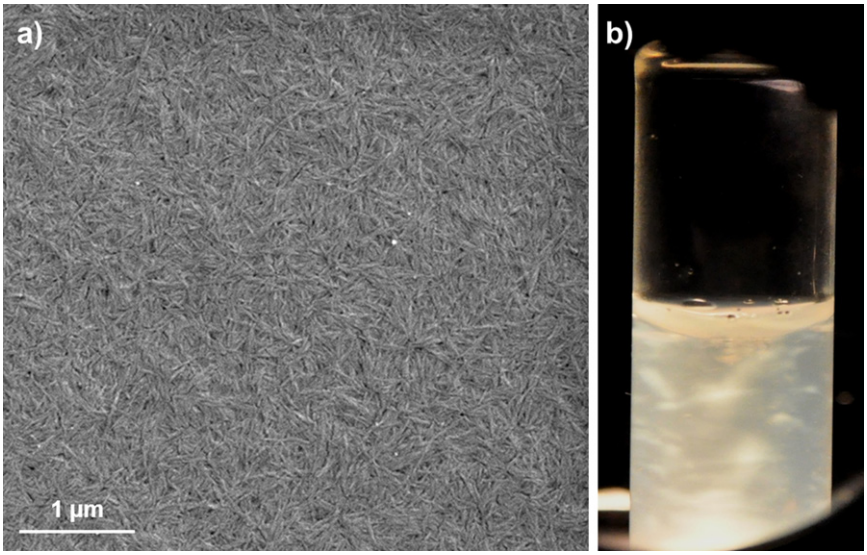

Fig. 1. FESEM image of freeze-dried surfactant modified cellulose nanocrystals (s-CNC) (a) and shear-induced polychromatic birefringence for s-CNC in a suspension of chloroform (b).

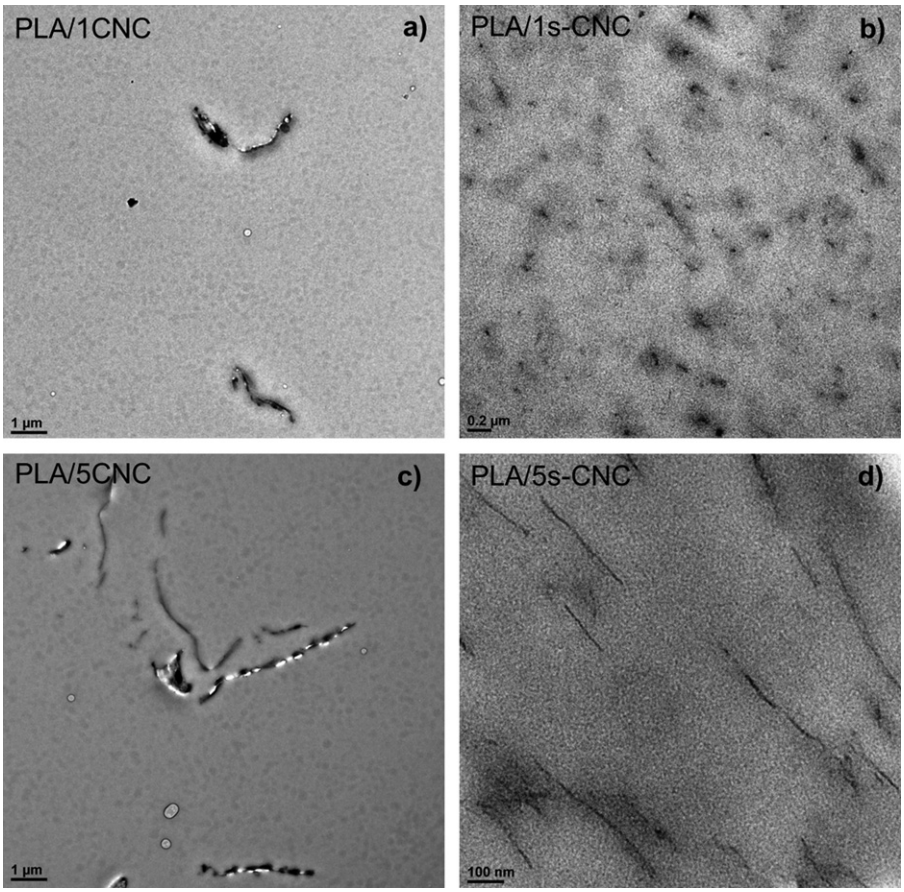

Fig. 2. TEM images of PLA systems at different content of un-modified (a and c) and surfactant modified (b and d) cellulose nanocrystals.

suggesting that the suspension contained a large number of single cellulose crystals, highlighting the success of the proposed modification process.

3.2. PLA nano-biocomposite morphology and crystalline structure

Nano-biocomposite morphological behaviour was analysed by TEM and the main results are reported in Fig. 2. For the binary PLA/1CNC and PLA/5CNC nanocomposites (Fig. 2a and c, respectively) it was observed that most of the crystals were flake like structure consisting of tightly packed cellulose structures. This cluster formation may indicate that pristine cellulose nanocrystals tend to agglomerate by hydrogen bonding and the nano-biocomposite processing used in this work is not strong enough to avoid this process. A different behaviour was detected for PLA/1s-CNC and PLA/5s-CNC (Fig. 2b and d, respectively). TEM analysis of these systems showed the good dispersion of s-CNC in the nanoscale, since well-defined single crystals were detected in the cross-section of both nanocomposites. Therefore it is concluded that the surfactant was able to cover the single crystals during the solvent casting process allowing a better dispersion of cellulose structures in the PLA matrix.

The structures of pure PLA polymer, cellulose nanocrystal powder, and PLA nano-biocomposites were characterized by wide angle X-ray scattering (WAXS) in order to study the effect of the nanocrystals type and content on the crystallinity of the PLA matrix. Fig. 3a shows WAXS curves for PLA and CNC. PLA only showed a wide diffraction band at $2\theta = 16.5^\circ$, giving the idea of the PLA amorphous nature. On the other hand, cellulose nanocrystals exhibited four main reflection peaks at $2\theta = 15.0^\circ$, 16.3°, 22.5° and 34.4° (this last less defined) relative to the cellulose I crystalline structure.

Fig. 3b shows the effect of cellulose nanocrystals content and modification on nano-biocomposites crystallinity. The peaks at $2\theta = 16.5^\circ$ and 22.4° were the most prominent, being indicative of the PLA and cellulose crystallinities, respectively. The WAXS curves for nanocrystals peaks at $2\theta = 15.0^\circ$ and 16.3°, were not identified at these low cellulose contents, being replaced by a broad shoulder at around $2\theta = 16^\circ$, typical of a predominant amorphous material. However, when the nanocrystals content increased to 5 wt.%, a steady increase in the intensity of the peaks at $2\theta = 22.5^\circ$ was observed in both, CNC and s-CNC based systems, suggesting again an increase in the overall crystallinity of the nano-biocomposites. The narrow peak at $2\theta = 16.5^\circ$ for the PLA/5CNC system and the presence of a shoulder at around $2\theta = 19^\circ$ for the PLA/5CNC and PLA/5s-CNC nano-biocomposites were indicative of the increased ability to crystallize of the modified-nanocrystal based systems (Hossain et al., 2012).

3.3. PLA nano-biocomposite permeability studies

Table 1 gathers the oxygen transmission rate (OTR) values and the water vapour permeability (WVP) coefficients of PLA and PLA nano-biocomposites reinforced with both unmodified CNC and surfactant modified s-CNC.

Reductions in OTR values with respect to the PLA film of ca. 9% in the case of un-modified CNC added at 1 wt.%, and of ca. 26% in s-CNC based systems, at the same percentage were detected. These results underlined the positive effect of the cellulose modification in the increase in barrier properties. This effect was confirmed for the PLA/5s-CNC films that showed the highest reduction in OTR values (ca. 48%). Moreover, a positive influence of cellulose content was revealed since the nano-biocomposites with 5 wt.% of cellulose

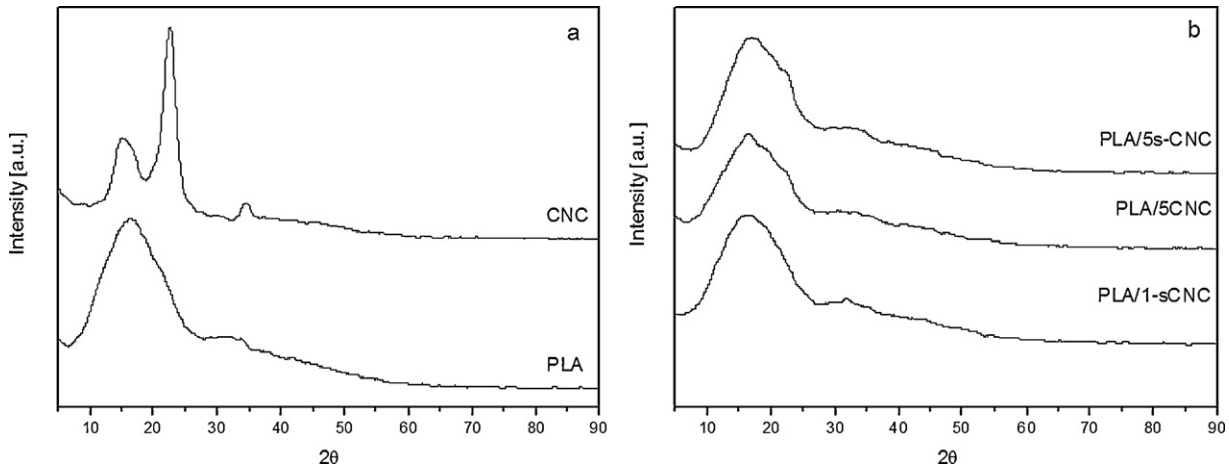

Fig. 3. Wide angle X-ray scattering of PLA pristine film and CNC powder (a) and of PLA nano-biocomposites at different content of un-modified and surfactant modified cellulose nanocrystals (b).

Table 1
Oxygen transmission rate and water vapour permeability coefficients for PLA and PLA nano-biocomposites.

Samples	OTR ($cm^3\ mm\ m^{-2}\ day^{-1}$)	Reduction in OTR (%)	Water vapour permeability $\times 10^{14}$ ($kg\ m\ m^{-2}\ s^{-1}\ Pa^{-1}$)	Reduction in WVP (%)
PLA	30.5 ± 1.0		1.04 ± 0.18	
PLA/1CNC	27.8 ± 0.1	9	1.05 ± 0.02	–
PLA/1s-CNC	22.7 ± 1.1	26	0.69 ± 0.01	34
PLA/5CNC	17.4 ± 1.4	43	0.99 ± 0.10	4
PLA/5s-CNC	15.8 ± 0.6	48	0.88 ± 0.13	15

also showed the best oxygen barrier properties for un-modified CNC based systems (reduction of ca. 43%). It is well known that the transport properties of gases through polymer films are strongly influenced by the tortuousity of their path, which is dependent on several factors including shape and aspect ratio of the filler, degree of exfoliation or dispersion, filler loading and orientation, adhesion to the matrix, moisture activity, filler-induced crystallinity, polymer chain inmobilization, filler-induced solvent retention and porosity (Sanchez-Garcia et al., 2008). Martino, Ruseckaite, Jiménez, and Averous (2010) also observed the improvement of PLA barrier properties due to a geometric factor which increased the tortuousity for gas molecules pathway to go through the film thickness as a consequence of the nanofiller addition. In our case, the s-CNC based nanocomposites are dispersed to a higher extent as showed in TEM analysis and possesses higher levels of crystallinity as show by the previous WAXS analysis, thus yielding a more efficient barrier effect (Fortunati, Armentano, Zhou, Puglia, et al., 2012).

Water vapour permeability coefficients are also reported in Table 1. These data are similar to others already reported (Sanchez-Garcia & Lagaron, 2010). Reductions of water permeability of ca. 34% were obtained for the cast films containing 1 wt.% of modified nanocrystals while a lower effect in the barrier properties for the PLA/1CNC nano-biocomposite was detected. The positive effect of cellulose modification in WVP barrier properties was also evident for this formulation. Lower reductions in water vapour permeability were detected in the case of nano-biocomposites reinforced with 5 wt.% of pristine CNC and modified s-CNC (4% and 15%, respectively, with respect to the value measured for PLA film). This particular result was already reported by Sanchez-Garcia et al. (2008). They indicated that the barrier properties to water of PLA nano-biocomposites containing cellulose microfibres were only reduced (by ca. 10%) in the sample containing 1 wt.% of the filler. Samples with 4 or 5 wt.% microfibres content showed no barrier improvements. It has been indicated that nano-biocomposites containing between 2 and 3 wt.% of nanocrystals exhibited the highest water and oxygen barrier. However, in this case, good oxygen barrier properties were also detected for nano-biocomposites with 5 wt.% of cellulose nanocrystals underlining the success of the solvent casting procedure and the reinforcement effect of both, pristine and modified nanocelluloses. Thereafter the barrier properties were significantly enhanced with the addition of modified cellulose compared to those nano-biocomposites with pristine cellulose at the same filler content. These results are in good agreement with previous studies concerning the crystallization kinetics of PLA-nanocellulose composites influenced by the filler nucleation effect (Fortunati, Armentano, Zhou, Puglia, et al., 2012).

3.4. PLA nano-biocomposite overall migration

Overall migration tests with simulants were carried out to determine the total amount of non-volatile substances that might migrate into foodstuff from PLA films (Schmidt et al., 2011). The results of overall migration levels of PLA and PLA nano-biocomposites, in ethanol 10% (v/v) and isooctane are shown in Fig. 4.

After 2 days of incubation at 20 °C, the maximum migration level in isooctane was 0.16 $mg\ kg^{-1}$ of simulant for PLA/5CNC. This value is much lower than the migration limits for food contact materials, 60 $mg\ kg^{-1}$ of simulant, established by the current legislation (Commission Directive, 2002/72/EC). By comparison of the total migration values for all samples in isooctane, there is a clear effect of the presence of cellulose nanocrystals that promote significantly the migration of the simulant. Neat PLA and PLA nano-biocomposites with 1 wt.% of cellulose showed negligible migration values. Samples with s-CNC had lower migration levels than those with CNC and this could be due to a better adhesion or interaction of the nanocrystals to the polymer matrix, as previously discussed.

In the case of migration in ethanol 10% (v/v), in general, higher migration levels were observed in comparison with isooctane, but all values were well below the overall migration legislative limits.

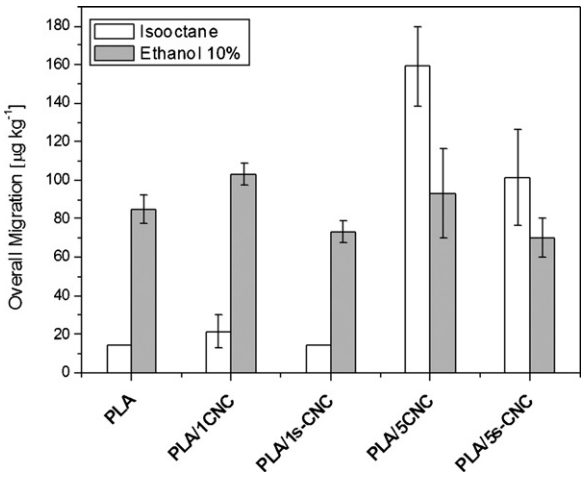

Fig. 4. Overall migration data in ethanol 10% (v/v) and isooctane for PLA and PLA nano-biocomposites.

Similar migration levels were observed for neat PLA and for the nano-biocomposites.

Thermodynamic properties, such as polarity and solubility, play an important role on migration due to interactions between the polymer, migrants and the food simulant (FS). If the migrant has a poor solubility in the FS it will be retained in the polymer matrix, while a simultaneous effect based on the high affinity between FS and the polymer could be also present leading to the absorption by the polymer matrix. In addition, sorption of certain organic solvents could cause swelling of the polymer matrix, thereby enlarging the gaps between the molecules and enhancing the additive migration (Zygoura, Paleologos, & Kontominas, 2011). In the case of this study, migration in isooctane was observed since the solvent might be absorbed in the polymer matrix, leading to the release of the small particles like nanocrystals and PLA degradation products.

3.5. Effect of ethanol interaction on PLA and PLA nano-biocomposites

The visual observation of PLA and PLA nano-biocomposite films immersed in ethanol 10% (v/v) for 10 days at 40 °C, revealed that the gross appearance of all these films changed after the overall migration test. The PLA nano-biocomposites were initially almost transparent. As the incubation time proceeded, samples lost their transparency and became whitish due to the water absorption (data not shown). The observed whitening during the incubation of the PLA nano-biocomposite films is assumed to be an effect of the molecular rearrangement caused by the increased mobility induced by the FS and it has been previously reported to be the result of accelerated spherulite formation (Sodergård & Stolt, 2002). For this reason, the surface microstructure and the thermal behaviour of PLA and PLA nano-biocomposite films, after the incubation in ethanol 10% (v/v), were investigated.

Fig. 5 shows the FESEM images of the binary PLA nano-biocomposites compared with the neat PLA film, before and after the overall migration test. After 10 days at 40 °C, a surface erosion with the appearance of holes on the PLA and PLA nano-biocomposites was detected since polylactide is a polyester resin, that are weak to alcohol (Mutsuga et al., 2008). Moreover, Fig. 5 highlights that holes about 10 μm in diameter were present on s-CNC nano-biocomposite surface, in particular in the PLA/5s-CNC system, while smaller holes were observed on neat PLA and PLA nano-biocomposites with un-modified CNC. A clear surface erosion with some fractures characterized the PLA/5CNC sample after the migration test. This behaviour could be the result of a higher ability of the system to interact with the polar solvent and it is in agreement with the low reductions detected in the WVP test.

The thermal behaviour of PLA nano-biocomposites after 10 days of incubation in ethanol 10% (v/v) was studied by DSC. The main thermal parameters are summarized in Table 2. The heating thermogram of the pristine PLA film showed the glass transition temperature (T_g) at about 45 °C, followed by the melting endotherm signal with its maximum (T_m) at about 151 °C. A similar behaviour was detected for all pristine PLA nano-biocomposites (Table 2). The cold crystallization peak was not clearly visible since although semi-crystalline, the PLA 3051D was reported to have slow nucleation and crystallization rates (Fortunati et al., 2011; Wu et al., 2007).

A different thermal behaviour was detected for the material after incubation. The heating thermograms displayed the glass-transition temperature, a well visible cold crystallization peak and the melting endothermal peak (data not shown). After 10 days of incubation the T_g increased for all the studied systems as the result of the annealing with the enthalpy relaxation peak and the cold crystallization became clearly visible in the first heating scan for all samples. The crystalline domains originated during the degradation process could act as cross-linking agents, hindering the motion of the polymer chains and consequently increasing the T_g value (De Paula, Mano, & Vargas Pereira, 2011). At low temperature additional endothermic shoulder upon melting (T'_m) characterized the PLA sample and PLA nano-biocomposites based on unmodified CNC (Table 2). The presence of multiple melting peaks in PLA is well known and has been related to the formation of different crystal structures (Yasuniwa, Sakamo, Ono, & Kawahara, 2008) or to lamellar populations with different perfection degrees (Kong & Hay, 2003) induced by the incubation conditions (Fortunati et al., 2011). Poly(lactic acid) can exhibit up to three possible crystal modifications (α, β and γ), depending upon the crystallization conditions. The crystal structure of α and β forms has been widely

Table 2
Thermal properties of PLA and PLA nano-biocomposites obtained from TGA measurements and DSC at the first heating scan before and after the overall migration test in ethanol 10% (v/v).

Samples		T_g (°C)	ΔH_m (J g^{-1})	T_m (°C)	T'_m (°C)	ΔH_{cc} (J g^{-1})	T_{cc} (°C)	T_{max} (°C)
PLA	Before incubation in ethanol 10% (v/v)	45.0 ± 2.0	25.8 ± 0.7	151.2 ± 0.5	–	–	–	364 ± 1
	After incubation in ethanol 10% (v/v)	55.2 ± 2.0	29.5 ± 2.0	151.7 ± 0.5	143.5 ± 0.5	24.3 ± 1.0	99.3 ± 1.0	365 ± 1
PLA/1CNC	Before incubation in ethanol 10% (v/v)	43.0 ± 1.0	30.7 ± 0.5	144.4 ± 1.0	–	–	–	356 ± 1
	After incubation in ethanol 10% (v/v)	55.6 ± 1.7	29.8 ± 0.3	151.7 ± 0.5	143.7 ± 0.3	23.6 ± 2.0	101.0 ± 1.9	362 ± 1
PLA/1s-CNC	Before incubation in ethanol 10% (v/v)	42.3 ± 0.4	30.7 ± 0.8	145.1 ± 0.5	–	2.7 ± 0.3	87.3 ± 0.5	353 ± 1
	After incubation in ethanol 10% (v/v)	55.5 ± 2.0	30.3 ± 1.4	150.2 ± 0.2	–	17.9 ± 0.5	82.7 ± 0.9	343 ± 3
PLA/5CNC	Before incubation in ethanol 10% (v/v)	43.0 ± 1.5	23.5 ± 0.5	145.6 ± 0.5	140.0 ± 1.0	–	–	361 ± 1
	After incubation in ethanol 10% (v/v)	57.0 ± 0.5	35.0 ± 2.0	151.5 ± 0.4	144.0 ± 0.4	26.8 ± 2.0	103.2 ± 0.5	357 ± 1
PLA/5s-CNC	Before incubation in ethanol 10% (v/v)	47.0 ± 1.0	32.9 ± 0.3	150.8 ± 0.5	146.2 ± 0.5	6.4 ± 0.2	91.9 ± 0.5	356 ± 1
	After incubation in ethanol 10% (v/v)	51.3 ± 0.5	39.4 ± 2.0	151.1 ± 0.5	–	18.4 ± 2.0	81.2 ± 2.0	362 ± 2

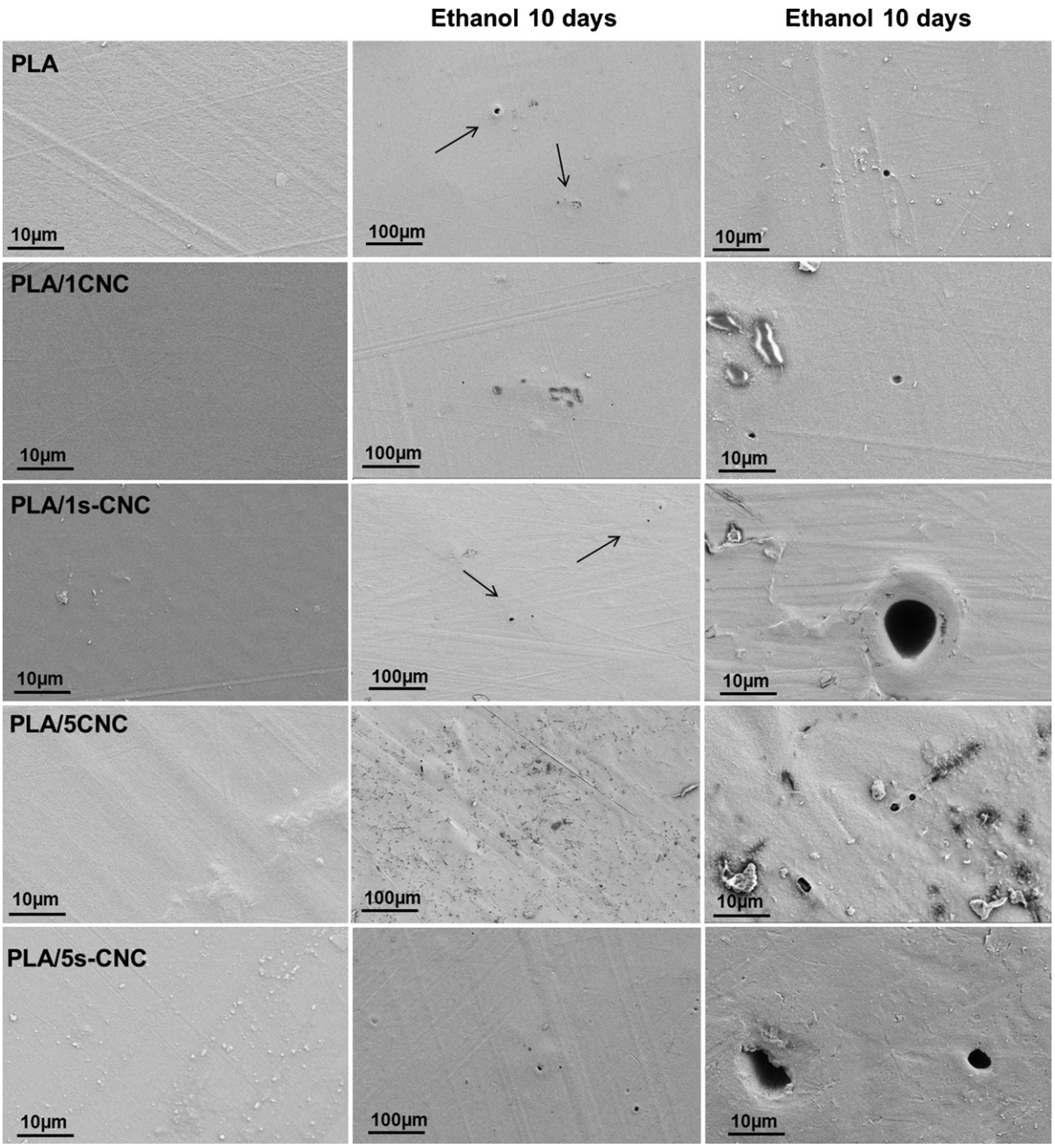

Fig. 5. Microstructure of PLA and PLA nano-biocomposites after 10 days of incubation in ethanol 10%.

investigated (De Santis & Kovacs, 1968; Eling, Gogolewski, & Pennings, 1982; Hoogsteen, Postema, Pennings, Ten Brinke, & Zugenmaier, 1990) highlighting that the β-structure melts at temperature about 10 °C below the melting temperature of the α-structure. From this observation they concluded that the PLA β-structure is some-what less stable than the α-structure. The phenomenon of multiple melting peaks was not detected in the case of s-CNC based systems where only one melting peak at around 151 °C was detected highlighting a higher thermal stability respect to neat PLA and PLA based CNC films. Moreover, when the surfactant modified cellulose (s-CNC) was added to PLA, the cold crystallization temperature decreased by approximately 17 °C. The interaction of PLA with the simulant, promotes a different arrangement of PLA molecular chains that influences the thermal behaviour of these systems.

The crystals forms of PLA are related to the crystallization temperature (T_c). Zhang, Tashiro, Tsuji, and Domb (2008) described that a crystal form named α′ form (a disordered form of α-PLA) is observed when polymer is crystallized at temperatures below 120 °C. These authors described that at $T_c < 100$ °C there is only one crystal form, i.e. α′. When the temperature increases, the α crystals start to appear and the amount of α′ crystals decreases, this is at temperatures 100 °C < T_c < 120 °C PLA crystallized in a combination of α and α′ phases.

The ability to reorganize the PLA structures is due to the chain flexibility, which is the result of the swelling of the amorphous phase and it is also due to the simulant diffusion through the polymer. In our case, the ability to re-crystallize during the first heating scan changed after the incubation in ethanol and the effect was also conditioned by the cellulose type. The nucleation effect is more

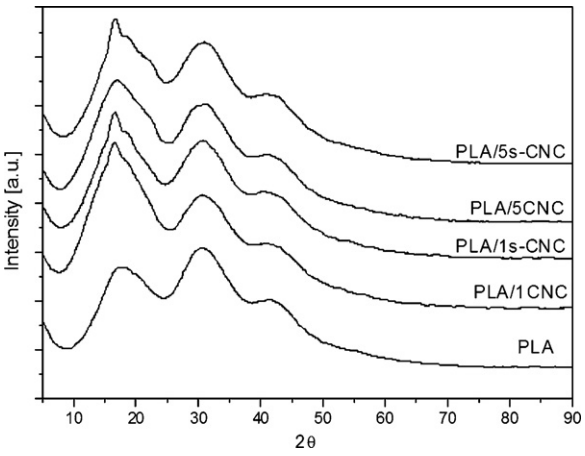

Fig. 6. Wide angle X-ray scattering of PLA and PLA nano-biocomposites after the overall migration test in ethanol 10% (v/v).

significant in s-CNC based systems, highlighting the influence of the modification on the final properties of the system.

In Fig. 6 the WAXS patterns of samples after incubation in ethanol 10% (v/v) for 10 days at 40 °C are observed confirming a dramatic change with respect to the pristine materials. Two peaks appear at 30.5 and 41.2° in all samples that can be attributed to a change in the crystallization form of PLA during incubation. This is in agreement with DSC results where the crystallinity of the samples changed after migration with the appearance of new crystals forms α and α′ but no increase of the overall crystallinity content was observed. In addition, samples with nanocellulose showed a sharpening of the peak at 16.6°, indicating that PLA suffered some structural rearrangement due to the presence of cellulose. The area of this peak was negligible in comparison with the amorphous halo, and consequently no increase in crystallinity was observed after migration tests (Ublekov, Baldrian, Kratochvil, Steinhart, & Nedkov, 2012).

Thermogravimetric analysis was also performed before and after the incubation with ethanol 10% (v/v) in order to investigate the degradation behaviour of these materials. The maximum degradation temperatures (T_{max}) of PLA and nano-biocomposites before and after the test are shown in Table 2. A complete weight loss with a single step was detected for neat PLA and all the studied composites before and after the incubation and no evident changes were detected in T_{max} value. This aspect highlights that at this step, the simulant penetration is able to induce modification in the polymer chain arrangement as previous discussed without affecting their pyrolysis temperature.

4. Conclusions

PLA nano-biocomposites reinforced with un-modified and surfactant modified cellulose nanocrystals were successfully prepared by solvent casting and the effect of cellulose modification and amount in the composite was deeply investigated.

TEM analysis showed the good dispersion of s-CNC in the nanoscale indicating that the addition of surfactant allowed the better dispersion of the CNC in the PLA matrix. The effect of cellulose nanocrystals in the PLA matrix was also investigated in term of barrier properties (oxygen transmission rate – OTR and water vapour permeability – WVP) and overall migration test in consideration of the intended application in food packaging. Reductions of 34% in WVP were obtained for films with 1 wt.% of s-CNC and good oxygen barrier properties were obtained for all nano-biocomposites, underlining the success of the solvent casting procedure and the reinforcement effect of cellulose. Moreover, the migration level of the studied nano-biocomposites were below the overall migration limits indicated in the current legislation in both non-polar and polar simulants, suggesting the possibility to use these systems in food packaging applications. Finally, the effects of ethanol (10%, v/v) on PLA and PLA nano-biocomposites after the overall migration tests were investigated. DSC and WAXS analyses underlined that the ability to re-crystallize of studied nano-biocomposites changed after the test and that the nucleation effect was most marked in s-CNC systems highlighting the influence of the modification on their final properties.

Acknowledgements

The authors gratefully acknowledge the financial support from the National Consortium of Materials Science and Technology (INSTM) and Spanish Ministry of Science and Technology (project MAT2011-28640-C02-01). We also acknowledge the Royal Institute of Technology of Stockholm, Sweden and in particular Prof. Lars A. Berglund.

References

Araki, J., Wada, M., & Kuga, S. (2001). Steric stabilization of a cellulose microcrystal suspension by poly(ethylene glycol) grafting. *Langmuir*, *17*, 21–27.

Auras, R., Kale, G., & Singh, S. P. (2006). Degradation of commercial biodegradable packages under real composting and ambient exposure conditions. *Journal of Environmental Polymer Degradation*, *14*, 317–334.

Bordes, P., Pollet, E., & Averous, L. (2009). Nano-biocomposites: Biodegradable polyester/nanoclay systems. *Progress in Polymer Science*, *34*, 125–155.

Commission Directive. (2002). Commission Directive 2002/72/EC relating to plastic materials and articles intended to come into contact with foodstuffs. *Official Journal of European Communities*.

Commission Regulation. (2011). Commission Regulation (EU) No 10/2011 on plastic materials and articles intended to come into contact with food. *Official Journal of European Communities*.

Cranston, E. D., & Gray, D. G. (2006). Morphological and optical characterization of polyelectrolyte multilayers incorporating nanocrystalline cellulose. *Biomacromolecules*, *7*, 2522–2530.

De Paula, E. L., Mano, V., & Vargas Pereira, F. (2011). Influence of cellulose nanowhiskers on the hydrolytic degradation behaviour of poly(D,L-lactide). *Polymer Degradation and Stability*, *96*, 1631–1638.

De Santis, P., & Kovacs, A. J. (1968). Molecular conformation of poly(S-lactic acid). *Biopolymers*, *6*, 299–306.

Eling, B., Gogolewski, S., & Pennings, A. J. (1982). Biodegradable materials of poly(L-lactic acid). 1. Melt-spun and solution-spun fibres. *Polymer*, *23*, 1587–1593.

EN-1186. (2000). Overall migration testing for packaging and other food contact materials. In *EN-1186 migration testing for food contact materials*.

Fleming, K., Gray, D. G., & Matthews, S. (2001). Cellulose Crystallites. *Chemistry-A European Journal*, *7*, 1831–1836.

Fortunati, E., Armentano, I., Iannoni, A., Barbale, M., Zaccheo, S., & Kenny, J. M. (2011). New multifunctional poly(lactide acid) composites: Mechanical, antibacterial, and degradation properties. *Journal of Applied Polymer Science*, http://dx.doi.org/10.1002/app.35039

Fortunati, E., Armentano, I., Zhou, Q., Iannoni, A., Saino, E., Visai, L., et al. (2012). Multifunctional bionanocomposite films of poly(lactic acid) cellulose nanocrystals and silver nanoparticles. *Carbohydrate Polymers*, *87*, 1596–1605.

Fortunati, E., Armentano, I., Zhou, Q., Puglia, D., Terenzi, A., Berglund, L. A., et al. (2012). Microstructure and nonisothermal cold crystallization of PLA composites based on silver nanoparticles and nanocrystalline cellulose. *Polymer Degradation and Stability*, http://dx.doi.org/10.1016/j.polymdegradstab.2012.03.027

Goussé, C., Chanzy, H., Cerrada, M. L., & Fleury, E. (2004). Surface silylation of cellulose microfibrils: Preparation and rheological properties. *Polymer*, *45*, 1569–1575.

Heux, L., Chauve, G., & Bonini, C. (2000). Nonflocculating and chiral-nematic self-ordering of cellulose microcrystals suspensions in nonpolar solvents. *Langmuir*, *16*(21), 8210–8212.

Hoogsteen, W., Postema, A. R., Pennings, A. J., Ten Brinke, G., & Zugenmaier, P. (1990). Crystal structure conformation and morphology of solution-spun poly(L-lactide) fibers. *Macromolecules*, *23*, 634–642.

Hossain, K. M. Z., Ahmed, I., Parsons, A. J., Scotchford, C. A., Walker, G. S., Thielemans, W., et al. (2012). Physico-chemical and mechanical properties of nanocomposites prepared using cellulose nanowhiskers and poly (lactic acid). *Journal of Material Science*, *47*, 2675–2686.

Jamshidian, M., Tehrany, E. A., Imran, M., Jacquot, M., & Desobry, S. (2010). Poly-lactic acid: Production, application, nanocomposites and release studies. *Comprehensive Reviews in Food Science and Food Safety*, *9*, 552–571.

Kong, Y., & Hay, J. N. (2003). Multiple melting behaviour of poly(ethylene terephthalate). *Polymer*, *44*, 623–633.

Martino, V. P., Ruseckaite, R. A., Jiménez, A., & Averous, L. (2010). Correlation between Composition Structure and Properties of Poly(lactic acid)/Polyadipate-Based Nano-Biocomposites. *Macromolecular Materials and Engineering*, *295*, 551–558.

Martino, V. P., Jiménez, A., Ruseckaite, R. A., & Avérous, L. (2011). Structure and properties of clay nano-biocomposites based on poly(lactic acid) plasticized with polyadipates. *Polymers for Advanced Technologies*, *22*, 2206–2213.

Martucci, J. F., & Ruseckaite, R. A. (2010). Three-layer sheets based on gelatin and poly(lactic acid). Part 1. Preparation and properties. *Journal of Applied Polymer Science*, *118*, 3102–3110.

Mutsuga, M., Kawamura, Y., & Tanamoto, K. (2008). Migration of lactic acid lactide and oligomers from polylactide food-contact materials. *Food Additives and Contaminants*, *25*, 1283–1290.

Petersson, L., Kvien, I., & Oksman, K. (2007). Structure and thermal properties of poly(lactic acid)/cellulose whiskers nanocomposite materials. *Composites Science and Technology*, *67*, 2535–2544.

Samir, M. A. S. A., & Dufresne, A. (2005). Review of recent research into cellulosic whiskers their properties and their application in nanocomposite field. *Biomacromolecules*, *6*, 612–626.

Sanchez-Garcia, M. D., Gimenez, E., & Lagaron, J. M. (2008). Mophology and barrier properties of solvent cast composites of thermoplastic biopolymers and purified cellulose fibers. *Carbohydrate Polymers*, *71*, 235–244.

Sanchez-Garcia, M. D., & Lagaron, J. M. (2010). On the use of plant cellulose nanowhiskers to enhance the barrier properties of polylactic acid. *Cellulose*, *17*, 987–1004.

Schmidt, B., Katiyar, V., Plackett, D., Larsen, E. H., Gerds, N., Bender Koch, C., et al. (2011). Migration of nanosized layered double hydroxide platelets from polylactide nanocomposite films. *Food Additives and Contaminants*, *28*, 956–966.

Sodergård, A., & Stolt, M. (2002). Properties of lactic acid based polymers and their correlation with composition. *Progress in Polymer Science*, *27*, 1123–1163.

Sturcova, A., Davies, G. R., & Eichhorn, S. J. (2005). Elastic modulus and stress-transfer properties of tunicate cellulose whiskers. *Biomacromolecules*, *6*, 1055–1061.

Schwach, E., Six, J. L., & Luc Averous, L. (2008). Biodegradable blends based on starch and poly(lactic acid): Comparison of different strategies and estimate of compatibilization. *Journal of Polymers and the Environment*, *16*, 286–297.

Turbak, A. F., Snyder, F. W., & Sandberg, K. R. (1983). Microfibrillated cellulose, a new-cellulose product: Properties, uses and commercial potential. *Journal of Applied Polymer Science Applied Polymer Symposium*, *3*, 815–827.

Ublekov, F., Baldrian, J., Kratochvil, J., Steinhart, M., & Nedkov, E. (2012). Influence of clay content onthe melting behaviour and crystal structure of non-isothermal crystallized poly(L-lactic acid)/nanocomposites. *Journal of Applied Polymer Science*, *124*, 1643–1648.

UNE 53097:2002 sheet materials – Determination of water vapour transmission rate – Gravimetric (dish) method.

Wang, N., Ding, E., & Cheng, R. (2007). Thermal degradation behaviors of spherical cellulose nanocrystals with sulfate groups. *Polymer*, *48*, 3486–3493.

Wu, D., Wu, L., Wu, L., Xu, B., Zhang, Y., & Zhang, M. (2007). Nonisothermal cold crystallization behaviour and kinetics of polylactide/clay nanocomposites. *Journal of Polymer Science Part B: Polymer Physics*, *45*, 1100–1113.

Yasuniwa, M., Sakamo, K., Ono, Y., & Kawahara, W. (2008). Melting behavior of poly(L-lactic acid): X-ray and DSC analyses of the melting process. *Polymer*, *49*, 1943–1951.

Zhang, J., Tashiro, K., Tsuji, H., & Domb, A. J. (2008). Disorder-to-order phase transition and multiple melting behaviour of poly(L-lactide) investigated by simultaneous measurements of WAXD and DSC. *Macromolecules*, *41*, 1352–1357.

Zygoura, P. D., Paleologos, E. K., & Kontominas, M. G. (2011). Changes in the specifics migration characteristics of packaging-food simulant combinations caused by ionization radiation: Effect of food simulant. *Radiation Physics and Chemistry*, *80*, 902–910.